Intrinsic, periodic and tunable metabolic dynamics: a scaffold for cellular coherence

Papagiannakis, Alexandros

Chapter 4

CDK and cAMP/PKA signalling tune the amplitude of the metabolic oscillator, thereby controlling cell cycle initiation or arrest

Alexandros Papagiannakis, Vakil Takhaveev, Matthias Heinemann

Molecular Systems Biology, Groningen Biomolecular Sciences and Biotechnology Institute, University of Groningen, Nijenborgh 4, 9747 AG Groningen, The Netherlands

Summary

The cyclin/CDK machinery, the cAMP/PKA pathway and the metabolic oscillator are known to form an intertwined network for the robust coordination of metabolism with the cell cycle in response to nutrient availability. Here we perform a small-scale genetic screening, using constitutive and conditional genetic perturbations, to investigate the effects of cAMP/PKA- and CDK-signaling on the metabolic oscillator. We show the amplitudes of the metabolic oscillations to strongly correlate with the cell cycle, and constitute an accurate predictor of cell cycle initiation. The cAMP/PKA pathway is not necessary for metabolism to oscillate, but stabilizes the amplitude of the noisy metabolic oscillator above the required threshold for cell cycle initiation in nutrient rich conditions. Dampened metabolic dynamics, either the result of poor nutrient conditions or mating pheromone induced CDK inhibition, activate the metabolic attenuator Rim15 for the robust arrest of the cell cycle in G1. Our results point towards the metabolic oscillator and the correlated dynamics, as potential targets for cell cycle manipulation against proliferative disorders.

Highlights

- Metabolic oscillations persist upon inhibition of the cAMP/PKA and CDK signaling and thus are autonomous.
- In the absence of cAMP/PKA and CDK signaling, the amplitude of the metabolic oscillations is dampened.
- In nutrient rich conditions, a positive feedback loop via cAMP/PKA signaling stabilizes the metabolic dynamics above the threshold for cell cycle initiation.
- The amplitude of the metabolic oscillations strongly correlates with cell cycle progression, and can be used to predict cell cycle initiation or cell cycle arrest.

Introduction

Through the course of the cell cycle, eukaryotes are confronted with different metabolic demands, such as for DNA replication in the S phase, or for cell wall synthesis during mitosis. Additionally, the cell cycle and metabolic processes of DNA replication and respiration, have been conjectured to be incompatible due to the production of reactive oxygen species during respiration that could damage DNA (Tu et al., 2005). Thus, for a timely provision of resources, or for temporal separation of incompatible processes, coordination between metabolism and the cell cycle seems necessary

Cell cycle-driven coordination of metabolism has been revealed, partly through research done on nutrient-limited synchronized yeast populations (Cai and Tu, 2012; Lloyd and Murray, 2005; Müller et al., 2003; Slavov and Botstein, 2011; Tu et al., 2005). For instance, a periodic cAMP/PKA and CDK activity have been suggested to drive the liquidation of stored carbon, thereby fuelling glycolysis and triggering the G1/S transition (Ewald et al., 2016; Zhao et al., 2016). However, interactions in the opposite direction were also found. The glycolytic flux-dependent metabolite acetyl-CoA has been shown to activate the expression of cell cycle components (e.g. Cln3) and growth-related genes (e.g. ribosomal), via the Gcn5/SAGA complex and the acetylation of histones (Cai et al., 2011; Shi and Tu,

2013). Going one step further, we recently found autonomous metabolite oscillations in single yeast cells, which occur in synchrony with but also without cell cycle progression (Papagiannakis et al., 2017). These metabolic oscillations adjust their frequency to the available nutrients and gate the cell cycle phases, thus setting the rate of division and orchestrating the transition between the cell cycle phases. It is tempting to speculate that an autonomously oscillating metabolism exists, which provides periodic triggers for cell cycle progression.

However, with the intricate interactions between metabolism, nutrient-sensing pathways and the cyclin/CDK machinery, it is hard to pinpoint the driver(s) behind these oscillations and to establish causality. Such research is further complicated by the dynamic nature of the involved processes, with certain interactions being functional only at certain moments during cell division (Cornelia Amariei, 2014; Machné and Murray, 2012; Tu et al., 2005), as well as the wide range of unspecific effects of metabolic perturbations, either applied at the genetic level (Deutscher et al., 2008) or by nutrient changes (Papagiannakis et al., 2017). Thus, to find out the minimal functional ingredients of an autonomously oscillating metabolism, it is important to disentangle cross-influences and expose the redundancy in the network.

An example of a network that connects metabolism and the cell cycle machinery is the cAMP/PKA/Rim15 pathway, integrating metabolic signals to control metabolic fluxes and to determine cell fate (Thevelein and de Winde, 1999). The central enzyme of the pathway, adenylate cyclase (Cyr1), synthesizes cAMP, which activates protein kinase A (PKA). Elevated Cyr1 activity leads to liquidation of storage carbon into glycolysis, fermentation and growth (Lee et al., 2013; Reinders et al., 1998). Adversely, absence of Cyr1 activity correlates with the accumulation of storage carbohydrates, respiration and a stationary phase metabolism (Pedruzzi et al., 2000; Smith et al., 1998). Next to its metabolic targets, cAMP signalling is known to deactivate the cyclins Cln1/2 (Baroni et al., 1994), while inhibiting the binding of the Whi3 translational inhibitor to the Cln3 mRNA (Mizunuma et al., 2013), thus granting a Cln3- and size-dependent START (Ferrezuelo et al., 2012; Schmoller et al., 2015; Talia et al., 2007), while inhibiting the anaphase promoting complex (APC1/3) for a robust separation of the early and late cell cycle (Kotani et al., 2016). While a periodic cAMP/PKA activity during the course of cell division has previously been

suggested (Müller et al., 2003) on the basis of cAMP measurements in cell-cycle synchronized populations, it is not clear how such an oscillating activity could emerge solely from the cAMP/PKA components and their interactions. Eventually, an autonomous metabolic oscillator (Papagiannakis et al., 2017) manifested via the oscillating concentration of key metabolites (e.g. FBP - (Sasidharan et al., 2012)) could entrain the cAMP/PKA activity. In fact, PKA was found to receive input from oscillating metabolites such as glucose-6-phosphate, fructose-1,6-bisphosphate, dihydroxyacetone-phosphate and glyceraldehyde-3-phosophate, via Ras (Peters, 2013). Overall, the cAMP/PKA/Rim15 pathway is embedded in an intertwined network, receiving input from and at the same time targeting metabolism.

Here, we performed a small-scale genetic screen in budding yeast to quantify the influence of cAMP/PKA- and CDK-signalling on the metabolic oscillator and the cell cycle. We either dynamically or statically removed network components, and observed the respective phenotypes on the single-cell level, including the dynamics of the metabolic oscillations, cell cycle progression, as well as the cellular physiology assayed on the population level. We found that the cAMP/PKA pathway is not necessary for metabolism to oscillate but stabilizes its amplitude in the presence of the Rim15 metabolic attenuator, facilitating cell cycle initiation. The conditional depletion of the Cdc28, the only CDK in yeast cells and inhibition target of the mating pheromone, elicited a similar metabolic response, i.e. dampening of the amplitude of the metabolic oscillator. Our data indicate the existence of a metabolic oscillator, the amplitude of which is strengthened by nutrient and cell cycle signalling pathways. Further, we found that the amplitudes of the metabolic oscillations strongly correlate with cell cycle initiation or arrest. Thus, the signalling pathways as well as the metabolic oscillator may serve as potential targets for cell fate manipulation or against proliferative disorders.

Identification of perturbation targets

As outlined above, metabolism together with the cAMP/PKA/Rim15 nutrient signalling and the cyclin/CDK machinery form an intertwined and network of metabolic pathways, transcriptional regulators and phosphorylation cascades. In search of central nodes and

perturbation targets for the investigation of the effects of cAMP/PKA- and CDK-signalling on the metabolic oscillator and the cell cycle, we present an overview of the respective network topology (Figure 1).

The adenylate cyclase, Cyr1, is a central node in the cAMP/PKA/Rim15 pathway (Thevelein and de Winde, 1999), integrating extracellular and intracellular signals to a uniform response, that of cAMP production and PKA activation. Cyr1 deletion alone disrupts the cAMP/PKA signalling cascade and is known to be lethal (Peeters et al., 2006; Zimmermann et al., 1998). One downstream target of PKA is the Rim15 kinase. Rim15 activates transcription via the PDS (post-diauxic shift) elements (Pedruzzi et al., 2000) and STREs (stress responsive elements) (Smith et al., 1998) (Figure 1), suppressing glycolysis and ribosomal biosynthesis, thus facilitating entry into the stationary phase (G0). Rim15 deletion is known to rescue the lethal *Cyr1Δ* phenotype (Reinders et al., 1998). The cAMP/PKA and Rim15 together can be considered an inhibitor/activator pair, where elevated cAMP production suppresses the Rim15 stress response and post-diauxic shift metabolism, when intracellular and extracellular nutrients are available. To investigate the effect of this pathway on the metabolic oscillator and the cell cycle, Cyr1 and Rim15 can be targeted independently or combined.

Another downstream target of PKA and Cdc28 is the neutral trehalase (Nth1), liquidizing trehalose into glycolysis at the G1/S transition (Figure 1) (Ewald et al., 2016; Zhao et al., 2016). Although it has previously been conjectured that PKA/CDK-induced cycles of trehalose liquidation could explain the periodic entrainment of metabolism during cell division (Futcher, 2006; Müller et al., 2003), they cannot account for the oscillating metabolism for the following reasons: (i) trehalose accumulation and utilization occurs only on slow growth conditions (François and Parrou, 2001; Guillou et al., 2004), such as glucose-limited continuous cultures (Müller et al., 2003) or during growth on ethanol (Ewald et al., 2016; Zhao et al., 2016). However, we have previously shown that metabolism oscillates also during aerobic fermentation (Papagiannakis et al., 2017). (ii) Yeast mutants unable to store trehalose and glycogen do not exhibit any significant cell cycle or cell size phenotype during growth on ethanol or glycerol (Zhao et al., 2016). However, given the metabolic targets of cyclin-dependent kinases, such as the cyclinB1/CDK1-mediated activation of mitochondrial respiration during the G2/M

transition described in mammalian cells (Wang et al., 2014), the yeast cyclin dependent kinase Cdc28 still constitutes an interesting perturbation target towards unravelling the interplay between metabolism and the cell cycle.

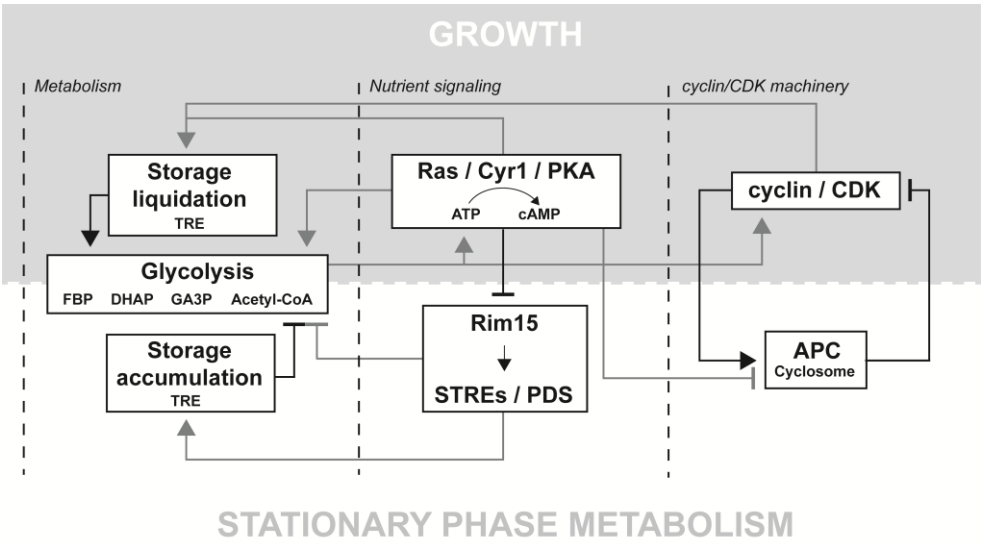

Figure 1: Metabolic pathways, nutrient signalling and the cyclin/CDK machinery form an intertwined network, for the robust coordination between the cell cycle and metabolism. According to the presented model, the cAMP/PKA pathway receives dynamic input from glycolytic intermediates (i.e. Fructose-1,6-bisphosphate - FBP, Dihydroxyacetone-phosphate - DHAP, Glyceraldehyde-3-phosphate - GA3P), the concentrations of which regulate the activity of Ras (Peters, 2013). Metabolism also provides input to the cyclin/CDK machinery, via the metabolite acetyl-CoA, which is known to epigenetically activate the expression of Cln3 at START (Cai et al., 2011; Shi and Tu, 2013). PKA and the CDK have been suggested to co-activate the enzyme neutral trehalase (Nth1), catalyzing the liquidation of trehalose (TRE) into glycolysis (Ewald et al., 2016; Zhao et al., 2016). Adversely, in the absence of cAMP signalling, Rim15 activates transcription via the stress responsive elements (STREs) and the post-diauxic shift (PDS) elements, suppressing glycolysis and activating trehalose accumulation (Pedruzzi et al., 2000; Smith et al., 1998). Finally, the anaphase promoting complex is known to be inhibited by high PKA activity (Kotani et al., 2016).

Means of perturbation and related experiments

In this study, we used different means of perturbation. Rim15 was deleted at the gene level. The auxin-inducible degron (AID) was used to conditionally and dynamically deplete essential proteins (Morawska and Ulrich, 2013; Nishimura et al., 2009). Cyr1 and Cdc28 were tagged with the auxin degron sequence at their C-terminal, for ubiquitination and proteasomal degradation upon the addition of the plant hormone auxin, in the presence of the plant F-box protein Os-TIR1. After the addition of auxin the targeted proteins were fully depleted within 25 min (Figure S1). Because the average doubling time of yeast during aerobic fermentation (10 gL^{-1} glucose) is 100 min, using the AID system we could generate deletion phenotypes within the duration of a single division cycle. Finally, the alpha factor was used as an additional way to perturb Cdc28 activity. The alpha factor is known to activate Far1, an inhibitor of the cyclin-dependent kinase, via the pheromone response pathway (Bardwell, 2004), a MAPK (Mitogen Activated Protein Kinase) phosphorylation cascade commencing from the pheromone receptor and its coupled G-proteins. Additionally, the alpha factor has been suggested to inhibit the adenylate cyclase (Cyr1) (Liao and Thorner, 1980; Valbuena and Moreno, 2010).

As a reporter of the oscillating metabolic activity we used the auto-fluorescence of the NAD(P)H, previously shown to oscillate in synchrony with, but also in the absence of cell division (Lloyd and Murray, 2005; Lloyd et al., 2002; Papagiannakis et al., 2017; Xu and Tsurugi, 2006). Fluorescently labelled Whi5 was used as a reporter of Cdc28 activity (Figure S2A-C) (Costanzo et al., 2004). Whi5 is an inhibitor of cell cycle transcription, which - in the absence of CDK activity – is sequestered in the nucleus during the G1 phase. At START, the active complex Cln3/Cdc28 phosphorylates Whi5 causing its sequestration into the cytoplasm, leading to cell cycle initiation (Figure S2A) (Ferrezuelo et al., 2012; Liu et al., 2015; Schmoller et al., 2015). NAD(P)H auto-fluorescence and Whi5 localization were measured in single yeast cells using epi-fluorescence microscopy (Figure S2B). A microfluidic dissection platform was used to cultivate single yeast cells (Huberts et al., 2013; Lee et al., 2012).

On the population level, we used flow cytometry to monitor the growth and morphological (cell size) effects of the applied perturbations. In addition, to determine changes in cell

physiology upon alpha factor addition, in the presence or absence of Rim15, the glucose uptake and ethanol production rates were determined from dynamic metabolite concentration measurements in the culture supernatant. Overall, combining different perturbation schemes, we screened for effects of cAMP/PKA- and CDK-signalling on the metabolic oscillator and the cell cycle.

Results

Results from perturbation experiments on the single cell and population level

In order to unravel the implications of cAMP signalling on the metabolic oscillator and the cell cycle we dynamically depleted the adenylate cyclase (Cyr1) using the AID system (Morawska and Ulrich, 2013; Nishimura et al., 2009). Upon Cyr1-AID depletion, all cells stopped dividing and were arrested in the G1 phase (Figures S3 & 2A), consistent with Cyr1 being essential (Peeters et al., 2006; Zimmermann et al., 1998) and with the presumed importance of cAMP signalling for the G1/S transition (Baroni et al., 1994; Futcher, 2006; Mizunuma et al., 2013; Müller et al., 2003). Focusing on the metabolic dynamics, we found that cells continued to exhibit metabolic oscillations even after Cyr1-AID depletion and cell cycle arrest, albeit with seemingly lower amplitudes (Figure 2A).

The downstream effector of the cAMP/PKA pathway, the Rim15 kinase, is known to suppress glycolysis and ribosomal biosynthesis in the absence of cAMP activity (Conrad et al., 2014; Pedruzzi et al., 2000; Smith et al., 1998). Consistent with the synthetic rescue of the *Cyr1Δ* lethal phenotype by deleting Rim15 (Reinders et al., 1998), in cells lacking Rim15 we found a significant fraction (40%) that continued budding upon Cyr1-AID depletion (Figure 2B). This fraction continued exhibiting metabolic oscillations with high amplitudes, contrary to the cells of the non-dividing fraction, which exhibited seemingly dampened metabolic dynamics (Figure 2B).

The experiments with the alpha factor (Figure 2C) yielded similar phenotypes as the experiments, in which we conditionally depleted Cyr1-AID (Figure 2A-B): Cells with Rim15 and exposed to alpha factor were arrested in the G1 phase (un-budded cells) and

exhibited dampened metabolic dynamics. In the absence of Rim15 (Figure 2C-top), two populations emerged after the addition of the mating pheromone. The dividing population exhibited high amplitude metabolic oscillations (Figure 2C-middle), in contrast to the arrested cells (Figure 2C-bottom) with seemingly dampened metabolic dynamics. Consistent with the pheromone induced CDK inhibition via the pheromone response pathway (Bardwell, 2004) and the here observed dampening of the metabolic dynamics after the addition of α-factor, also when we conditionally depleted the Cdc28 using the AID mechanism (Morawska and Ulrich, 2013; Nishimura et al., 2009), we found cells to exhibit dampened metabolic oscillations (Figure 2D).

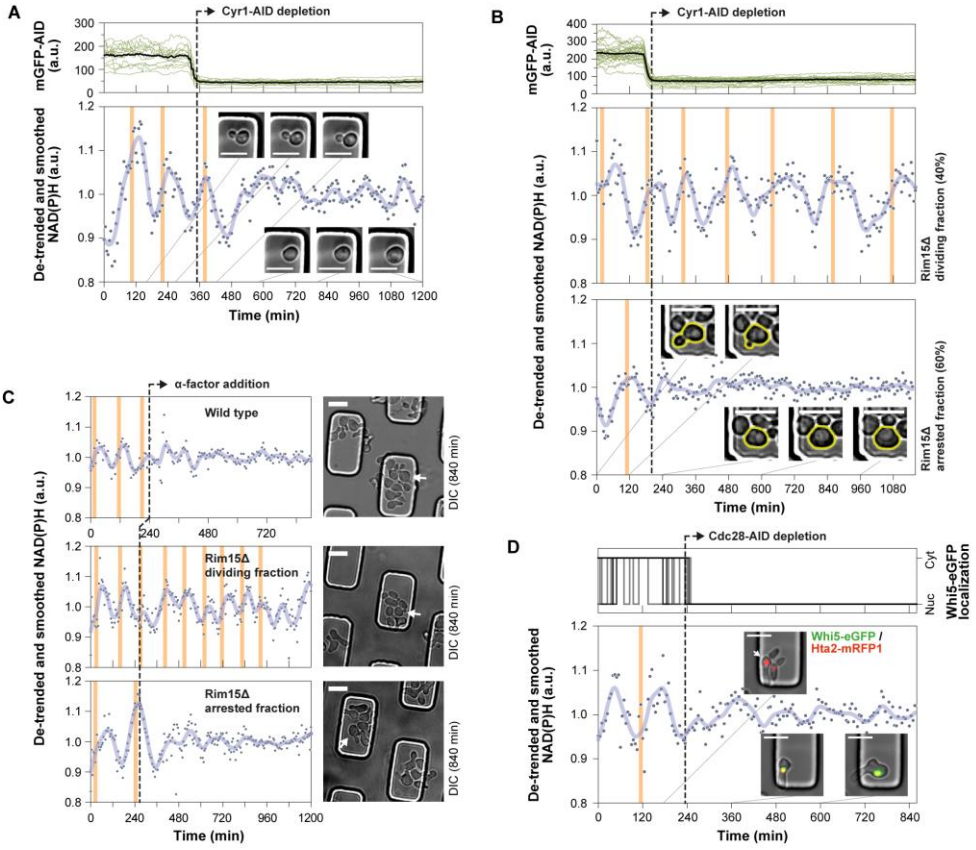

Figure 2: Results from the single cell perturbation experiments. Exemplary cells are presented for each perturbation experiment and subpopulation, including the metabolic (NAD(P)H) and cell cycle (budding, Whi5 localization) dynamics, as well as microscopy images (scale bars, 10 µm). All

experiments were performed with the microfluidic dissection platform for yeast. **(A)** Cyr1-AID was depleted using the auxin inducible degron. In order to determine the depletion dynamics of the adenylate cyclase, in the same experiment and the same microfluidic device we loaded control cells expressing mGFP tagged with the auxin degron sequence (mGFP-AID) and monitored their GFP dynamics. We have confirmed that the mGFP-AID can be used to estimate the Cyr1-AID depletion dynamics (Figure S1). Microscopy images confirm the cell cycle arrest in the G1 phase (cell without bud after Cyr1-AID depletion, see also Figure S2). Vertical orange lines correspond to budding. **(B)** As in Fig. 1A, also here we loaded mGFP-AID cells in the same microfluidic device to monitor the Cyr1-AID depletion dynamics in the *Rim15Δ* cells. Upon depletion of the adenylate cyclase and in the absence of Rim15 two populations emerge: a dividing population (approx. 40%) and a non-dividing population (approx. 60%). **(C)** Wild type (top) and *Rim15Δ* (middle and bottom) single cells before and after the addition of α-factor. Wild type cells (top) are arrested in the G1 phase after the addition of the mating pheromone adopting the shmoo phenotype (microscopy figure). In the *Rim15Δ*, we observe a dividing fraction of cells (middle), resembling exponentially growing unperturbed cells, and an arrested fraction (bottom) adopting the shmoo phenotype. **(D)** A single cell before and after the depletion of Cdc28-AID, signaled by the sequestration of Whi5-eGFP into the nucleus (as in Figure S2A-C). After the depletion of Cdc28-AID metabolic oscillations persist yet with seemingly lower amplitudes.

We confirmed the difference in the response of the wild type and the *Rim15Δ* cells to the addition of the mating pheromone also on the population level: First, analyzing the whole-population growth rates by flow cytometry after the addition of the mating pheromone, we found that in contrast to the wild type population which was almost completely growth arrested approaching a growth rate of 0 h^{-1}, in the absence of Rim15 cells achieved a higher population-averaged growth rate (approximately 0.1 h^{-1}) (Figure 3A), consistent with the incomplete cell cycle arrest in the *Rim15Δ* cells, and the existence of growing cell fractions that we found (Figure 2C).

Second, we focused on cell morphology. The α-factor induces the formation of mating projections upon cell cycle arrest, commonly known as the shmoo phenotype (Bardwell, 2004), resulting in bigger and polarized cells (cf. images in Figure 2C). Using flow-cytometry and the forward scatter as a proxy of cellular morphology we were able to discern between growing (mothers and daughters) and arrested (shmoo) cells (Figure 3B-C). Already 2.5 hours after the addition of the mating pheromone we could distinguish a growing fraction of dividing (non-shmooing and thus small) *Rim15Δ* cells (Figure 3C), in contrast to the wild type cells, which were all arrested (Figure 3B). By dividing the numbers of arrested cells prior and at different times after the addition of the mating

pheromone, we found a constantly increasing fraction of growing cells (after the α-factor addition) in the absence of Rim15, but not in the wild type cells (Figure 3D). These population level analyses based on a much larger number of cells confirmed the results on the two distinct phenotypes in the Rim15 deletion mutant as determined from the microfluidics experiments with much less analysed cells.

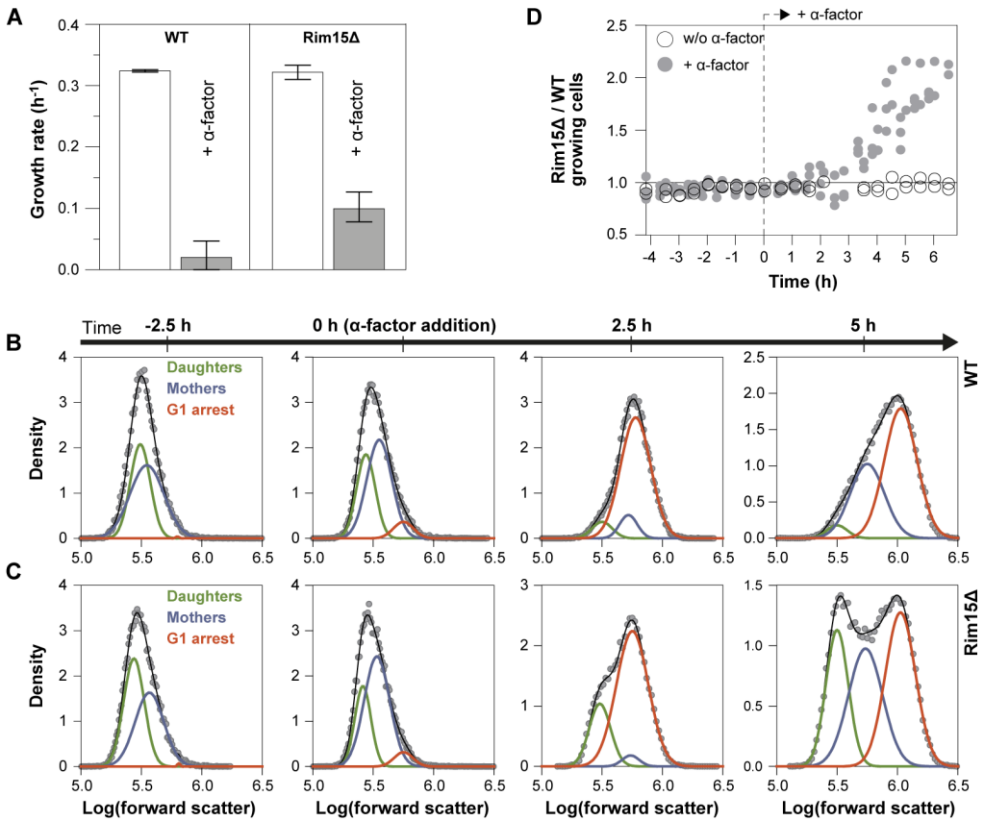

Figure 3: Phenotypic bistability, with dividing and G1-arrested population fractions, upon the addition of alpha factor in *Rim15*Δ cells. (A) The average growth rates (error bars: range of values) measured in wild type and *Rim15Δ* populations grown in the absence (2 biological replicates per strain) or in the presence of the mating pheromone (5 biological replicates per strain). **(B-C)** The Gaussian distributions of the daughter (green), mother (blue) and G1 arrested (red) cells, separated on the basis of their forwards scatter, prior and after the addition of α-factor (at 0 h), in wild type **(B)** or *Rim15Δ* **(C)** cells. A sum of three Gaussians (black line) was fitted to the entire population to determine the contribution of the three cell fractions. The mean logarithms of the forward scatter (fsc) of the daughter ($\log(fsc)_{daughters}$ = 5.45±0.05) and the mother ($\log(fsc)_{mothers}$ = 5.63±0.13) cells was

determined on the basis of exponentially growing unperturbed cultures and was fixed within the specified bounds during the fitting. The G1 arrested cells after the addition of the mating pheromone adopt the shmoo phenotype and are thus bigger than the corresponding mother cells ($\log(fsc)_{arrested} > 5.75$). **(D)** The number of dividing cells (daughters + mothers) in the *Rim15Δ* population, as determined from the fitted Gaussians, divided over the number of wild type growing cells, prior and after the addition of α-factor (grey markers), or during unperturbed growth in the absence of the mating pheromone (white markers).

Table 1: Overview of the applied perturbations and their effects on metabolism as well as the cell cycle. The auxin-inducible degron (AID) was used to conditionally deplete the essential adenylate cyclase (Cyr1) and cyclin dependent kinase (Cdc28). Rim15 was knocked out (KO) from the genome. The amplitudes of the metabolic oscillations were determined in single cells on the basis of the oscillating NAD(P)H signal. Metabolic oscillations were confirmed in all experiments by visual inspection. Budding was determined by microscopy or development of cell size and counts as determined by flow-cytometry were used to distinguish between growing and arrested cells.

Perturbation target(s)	Pathway(s)	Method(s)	NAD(P)H oscillations	Amplitude	Cell cycle
Cyr1	cAMP/PKA	AID	Yes	Dampened	Arrest
Cyr1 Rim15	cAMP/PKA	AID KO	Yes	Bistability Amp/Damp	Bistability Growth/Arrest
Cdc28 Cyr1	Cyclin/CDK cAMP/PKA	α-factor	Yes	Dampened	Arrest
Cdc28 Rim15	Cyclin/CDK cAMP/PKA	α-factor KO	Yes	Bistability Amp/Damp	Bistability Growth/Arrest
Cdc28	Cyclin/CDK	AID	Yes	Dampened	Arrest

The results from our perturbation experiments can be summarized into three main findings: (i) metabolic oscillations persisted even in the absence of cAMP and CDK signalling consistent with the previously conjectured autonomous nature of the metabolic oscillator, (ii) the metabolic dynamics were dampened in the absence of cAMP or CDK signalling, (iii) deletion of Rim15 generates phenotypic bistability in the absence of cAMP signalling or upon the addition of alpha factor, including a dividing cellular fraction with enhanced metabolic dynamics, and a G1-arrested cellular fraction with dampened metabolic oscillations. An overview of the applied perturbations and their observed effects on metabolism and the cell cycle is provided in Table 1.

The metabolic dynamics set a threshold between cell division and cell cycle arrest.

In our single cell perturbation experiments, we witnessed that every time the cell cycle was arrested, independently of the applied perturbation (Cyr1-AID depletion, Cdc28-AID depletion or α-factor addition), the metabolic oscillations as measured via NAD(P)H were dampened. To establish a correlation between the metabolic dynamics and the cell cycle, we needed to quantify the metabolic dynamics. For this purpose, we used the standard deviation of the NAD(P)H signals as an unbiased proxy of the amplitude of the metabolic oscillations. The standard deviation was estimated on the basis of single-cell NAD(P)H signals, after they were corrected for the low frequency noise by dividing over a fitted smoothing spline (p=1e-07, for all single cells).

Our results show a strong correlation between the metabolic dynamics and the cell cycle (division or arrest) (Figure 4A). The standard deviation of the single cell NAD(P)H signal sets a clear threshold between cell division and cell cycle arrest, independently of the applied perturbation. Enhanced NAD(P)H amplitudes (SD > 0.04) are predictive of cell cycle initiation, whereas attenuated metabolic amplitudes (SD < 0.04) are predictive of cell cycle arrest (Figure 4A). This is not the first time a metabolic threshold is identified between dividing and arrested cells. We have previously shown that the frequency of the metabolic oscillator is also a reliable predictor of cell cycle initiation (Papagiannakis et al., 2017), which can be used robustly distinguish between dividing and quiescent cells under nutrient limited conditions (0.01 gL^{-1} glucose). In fact, when found that the amplitude of the

metabolic oscillator can indeed also be used to distinguish between dividing and quiescent non-dividing cells, during respiratory growth on 0.01 gL^{-1} (Figure 4B).

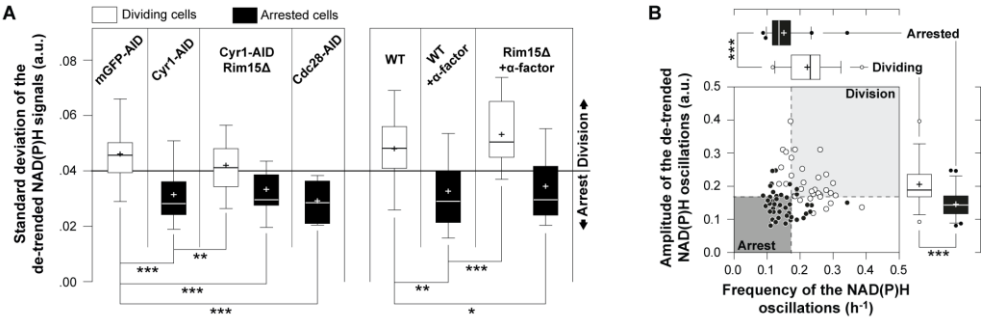

Figure 4: The frequency and the amplitude of the metabolic oscillations correlate with cell division or cell cycle arrest. (A) The standard deviation of the de-trended NAD(P)H signals was used as an unbiased proxy of the amplitude of the metabolic oscillator. The distribution of the standard deviations are presented (error bars 95% CI, + mean) from (left to right) 41 control cells (mGFP-AID depleted), 19 single cells after Cyr1-AID depletion in the presence of Rim15, 39 Rim15Δ single cells (18 dividing and 21 arrested) after Cyr1-AID depletion, 7 arrested cells after the conditional depletion of Cdc28-AID, 25 control cells (wild-type cells in the absence of α-factor), 24 arrested wild-type single cells after the addition of α-factor and 29 *Rim15Δ* cells after the addition of alpha factor (12 dividing and 17 arrested). Kruskal-Wallis significance test, Dunns post-test, * $p<0.05$, ** $p<0.01$, *** $p<0.001$. **(B)** The frequencies of 35 metabolic oscillations from an equal number of dividing cells (white markers), and the frequencies of 47 metabolic oscillations in the absence of cell division from 19 quiescent cells (black markers) of cells grown on 0.01 gL^{-1} glucose. Frequencies were estimated as the inverse of the time between consecutive troughs. The amplitudes of the oscillations were estimated by subtracting the average NAD(P)H level between two consecutive troughs from the NAD(P)H level at the intermediate peak. The distributions of the estimated frequencies and amplitudes are plotted in the corresponding box plots (whiskers: 5-95 percentile, cross: mean). The lower 25 percentiles of the measured amplitudes and frequencies in dividing cells were used to draw the respective thresholds (dotted lines) between cell division and cell cycle arrest (Mann-Whitney test, *** $p < 0.001$). All NAD(P)H signals were de-trended by dividing over fitted smoothing splines ($p = 1e\text{-}07$).

Here we show that cell cycle arrest requires the attenuation of the metabolic dynamics, which can be achieved via the inhibition of CDK or cAMP signalling (Figure 4A, Table 1). Our findings justify the interconnectivity between the metabolic oscillator, the cAMP/PKA pathway and the cyclin/CDK machinery, but also expose the redundancy in the network.

The cAMP/PKA pathway is not necessary for cell cycle initiation or pheromone mediated cell cycle arrest, but contributes to the robustness of both process, for a uniform metabolic and cell cycle response in the population.

The cAMP/PKA pathway establishes positive feedback to the metabolic dynamics and stabilizes the amplitude of the metabolic oscillations above the critical threshold for cell cycle initiation.

The cAMP/PKA pathway is thought to provide a molecular link between metabolism and the cell cycle. According to the "finishing kick to START" hypothesis (Futcher, 2006), developed on the basis of metabolite data from synchronized nutrient-limited cultures (Lloyd and Murray, 2005; Müller et al., 2003; Tu et al., 2005), elevated cAMP levels and PKA activity during the late G1 phase trigger the liquidation of trehalose into glycolysis, causing the onset of a fermentative metabolism and enhanced protein synthesis, until the trehalose reserves are depleted. As a result, the early cyclin production rates increase beyond their fast degradation, triggering cell cycle initiation and START.

However, our results contradict the "finishing kick to START" hypothesis" for two reasons: First, we found metabolism to continue to oscillate in Cyr1-AID depleted and cell cycle arrested cells, yet with lower amplitudes (Figures 2A & 4A). Second, when Cyr1-AID was conditionally depleted in the absence of the Rim15 kinase, i.e. the downstream target of PKA, we witnessed a significant fraction (40%) of normally dividing cells with normal metabolic dynamics (NAD(P)H SD > 0.04) (Figures 2B & 4A). Our results are consistent with the recent finding that yeast mutants, unable to synthesize storage carbohydrates, did not exhibit any growth defect or specific phenotype (Zhao et al., 2016). Thus, we show that the periodic entrainment of carbon storage metabolism by the cAMP/PKA pathway is not necessary for the metabolic oscillations or their coordination with the cell cycle.

Instead, the normal cell cycle progression and normal metabolic amplitudes (NAD(P)H SD > 0.04) that we observed in a significant fraction of the *Rim15Δ* cells, after the addition of α-factor and the conditional depletion of Cyr1-AID, suggests that Rim15 operates as a metabolic attenuator, robustly dampening the metabolic dynamics, which leads to cell cycle

arrest in the absence of cAMP signalling. In fact, confirming the metabolic role of Rim15, we found that the *Rim15Δ* cells yielded more ethanol per glucose molecule after the addition of alpha factor, as compared to wild type arrested cells (Figure 5A. Taking these observations together, we think that an oscillatory activity of cAMP/PKA – eventually induced by weak autonomous metabolic oscillations – dynamically activates Rim15 activity, which in turn dynamically impacts metabolism, thus together forming a positive feedback loop results in strengthened metabolic amplitudes (Figure 5B).

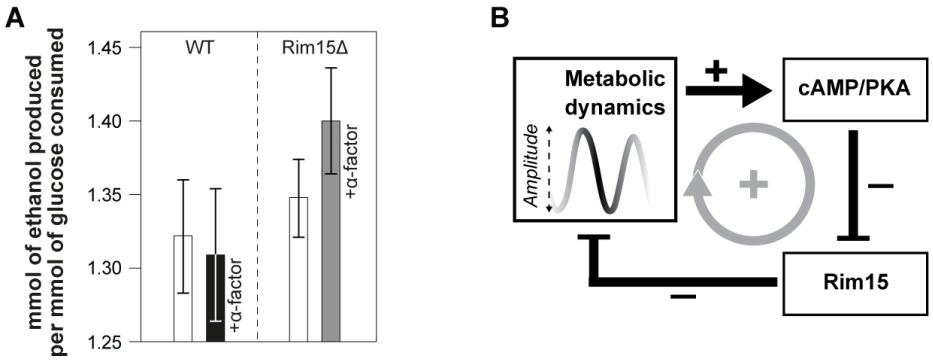

Figure 5: Rim15 is a metabolic attenuator, required for the robust pheromone induced cell cycle arrest. (A) The average ethanol yield measured in populations of wild type and *Rim15Δ* cells grown in the presence or the absence of the mating pheromone. Linear regression were fitted to data describing the amount of ethanol production per glucose production, both measured in the supernatant of the cultures. One linear regression was fitted to data from two biological replicates per strain and condition. The error bars represent the standard error of the slope of the fitted linear regression. **(B)** The cAMP/PKA/Rim15 pathway establishes a positive feedback loop on the metabolic dynamics. Metabolic dynamics activate cAMP signalling, thus strongly inhibiting the metabolic attenuator Rim15, and maintaining high amplitude oscillations. Reduced metabolic dynamics, insufficient to trigger cAMP signalling, activate the metabolic attenuator Rim15, which further dampens metabolism for a robust cell cycle arrest. The robust attenuation dynamics and cell cycle arrest is also be achieved by direct inhibition of the cAMP/PKA module, for instance by conditionally depleting Cyr1-AID.

The fact that we also observed strong metabolic oscillations in the absence of Cyr1 and Rim15 suggests that the positive feedback loop is not necessary to generate metabolic dynamics effective for cell cycle initiation (SD > 0.04). Adversely, our finding that a fraction of *Rim15Δ* cells was arrested in the absence of Cyr1, under rich nutrient conditions

($10gL^{-1}$ glucose), reveals stochasticity in the dynamics of the metabolic oscillator. In the absence of cAMP/PKA/Rim15 signaling this metabolic stochasticity is expressed as phenotypic bistability, due to the minimal metabolic threshold (SD = 0.04) required for cell cycle initiation. Overall we conclude that in nutrient rich conditions the cAMP/PKA/Rim15 positive feedback loop enhances and stabilizes the metabolic dynamics above the effective threshold for START, eliminating stochasticity in the metabolic and thus the cell cycle process.

The alpha factor arrests the cell cycle by dampening the metabolic dynamics

We have found that also the mating pheromone reduces the amplitude of the metabolic oscillator (Figure 6A) in a Rim15- and thus cAMP/PKA-dependent manner (Figure 2C), similarly to the conditional depletion of the adenylate cyclase (Figures 6A and 2A-B), leading to cell cycle arrest. Still, it remains unclear how the α-factor inhibits the cAMP/PKA pathway. Two models of mating pheromone-induced cAMP/PKA inhibition are possible: The "direct model of cAMP/PKA inhibition" (Figure 6B) is based on an old finding according to which the α-factor directly inhibits the adenylate cyclase (Liao and Thorner, 1980). Adversely, the mating pheromone could indirectly affect the cAMP/PKA activity, via the pheromone response pathway (Bardwell, 2004) and Cdc28 inhibition ("indirect model of cAMP/PKA inhibition" – Figure 6B). This could go as follow: the alpha factor inhibits CDK, which has also targets in metabolism (e.g. mitochondrial respiration), which in turn could affect cAMP/PKA through its input from metabolism, for instance through flux signalling metabolites (e.g. FBP). The thereby altered cAMP/PKA activity would lead to an activation of the Rim15 kinase, and would result in attenuation of metabolism.

The dampened metabolic oscillations in the Cdc28-AID depleted cells (Figure 4A & 6A), similarly to Cyr1-AID depletion or the addition of α-factor, confirm the metabolic function of CDK in yeast, and the support the "indirect model of cAMP/PKA inhibition" by the mating pheromone (Figure 6B). However, we cannot exclude the possibility that the mating pheromone targets the cAMP/PKA pathway both indirectly via Cdc28 and metabolism, as well as by directly inhibiting Cyr1 (Figure 6B).

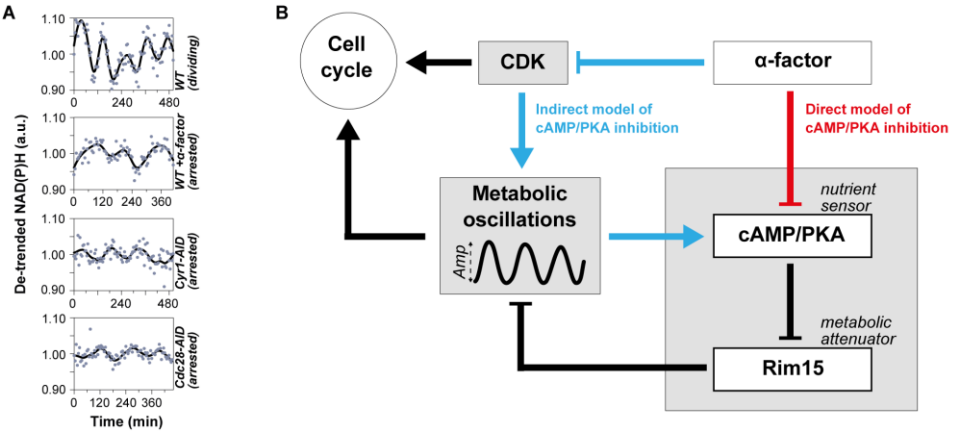

Figure 6: Reconstructed network topology derived from our single cell and population level perturbation experiments. (A) De-trended NAD(P)H oscillations from four exemplary single cells, including a control cell dividing normally on high glucose (top), a G1 arrested cell after the addition of α-factor, a G1 arrested cell after the conditional depletion of Cyr1-AID, and a cell cycle arrested cell after the conditional depletion of Cdc28-AID (bottom). **(B)** From our results we derive an interaction network topology between the metabolic oscillator, the cAMP/PKA/Rim15 pathway and the cyclin/CDK machinery, altogether contributing to cell cycle regulation. The cAMP/PKA/Rim15 pathway consists of (i) a sensory domain (cAMP/PKA) integrating signals from the autonomous (weak) metabolic oscillator and (ii) the attenuator module (Rim15) which reduces the metabolic dynamics in the absence of cAMP signalling. The mating pheromone inhibits the cAMP signalling indirectly (blue connections), via inhibiting Cdc28 consequently inhibiting metabolism, and possibly also directly (red connections) inhibiting Cyr1.

Discussion

In our small-scale genetic screening we have gained insight on the interactions between the metabolic oscillator, the cAMP/PKA pathway and cyclin/CDK machinery, as well as the emergent coordination between metabolism and the cell cycle. Here we show that the cAMP/PKA driven cycles of carbon storage accumulation/liquidation are not necessary for cell division or an oscillating metabolism. Our data expose the redundancy of the cAMP/PKA pathway, but most importantly suggest its role in removing noise from the metabolic dynamics. The adenylate cyclase (Cyr1) integrates signals from a periodic metabolism and the oscillating concentrations of glycolytic intermediates (e.g. FBP) via its

Ras activator (Peters, 2013), and thus functions as a sensor of the metabolic dynamics (Figure 6B). The Rim15 kinase constitutes the attenuation module (Figure 5B), which inhibits glycolysis and protein synthesis (Pedruzzi et al., 2000; Smith et al., 1998) when the sensory domain reports a "slow" metabolism (absence of PKA activity), either as a result if poor nutrient conditions, or after the addition of the mating pheromone, for the robust cell cycle arrest in G1. Adversely, in nutrient rich conditions, the cAMP/PKA pathway establishes a positive feedback to the metabolic dynamics (Figure 5B), stabilizing their amplitude above the effective threshold for cell cycle initiation, for a robust cell cycle initiation. If the metabolic sensor-attenuator pair (cAMP/PKA/Rim15) is removed altogether, then the cells are prone to the noise in the metabolic dynamics, occasionally escaping cell cycle arrest even upon the addition of the mating pheromone.

Here, we show a strong correlation between the amplitude of the metabolic oscillations and the cell cycle. Our findings are reminiscent of the previously conjectured metabolic checkpoint at START (Jones et al., 2016; Lee and Finkel, 2013; Schieke et al., 2008), controlling the G1/S transition in coordination with enhanced mitochondrial potential and bioenergetics, or the metabolic flux dependent expression of Cln3 triggering START (Cai et al., 2011; Shi and Tu, 2013). We identify this checkpoint as a threshold in the NAD(P)H dynamics, namely the frequency and the amplitude of the metabolic oscillations, which needs to be surpassed for cell cycle initiation. The same metabolic threshold is responsible for the emergence of two sub-populations, a dividing and a non-dividing one, during respiratory growth on low glucose (0.01 gL^{-1}) or upon the addition of alpha factor in the absence of the metabolic attenuator Rim15.

The metabolic oscillator constitutes a prime target for cell cycle regulation. Thus, it is not surprising that Cdc28 has an effect on the metabolic dynamics. In fact, metabolic functions have previously been attributed to the cyclin/CDK machinery. In mammalian cells, CDK1 has been shown to localize in mitochondria, phosphorylating components of the respiratory chain, enhancing mitochondrial respiration and accelerating the G2/M transition (Wang et al., 2014). The yeast CDK (Cdc28) has been suggested to co-activate the neutal trehalase together with the cAMP/PKA pathway (Ewald et al., 2016; Zhao et al., 2016), promoting the liquidation of trehalose into glycolysis at START. However, this has been identified as a secondary interaction. First, trehalose storages are almost empty during fermentative

growth on high ($10gL^{-1}$) glucose (François and Parrou, 2001; Guillou et al., 2004), whereas yeast mutants unable to store trehalose or glycogen did not exhibit any specific phenotype or growth defects during exponential growth on ethanol or glycerol (Zhao et al., 2016). It still remains unknown how the CDK activity stabilizes the amplitude of the metabolic oscillations during fermentative growth.

The Warburg effect provides a widely cited connection between metabolism and the cell cycle (Diaz-Ruiz et al., 2011; Vander Heiden et al., 2009). Cancer cells exhibit increased rates of glycolysis, secreting large amounts of fermentation products (e.g. lactate), even in the presence of oxygen. Adversely, somatic non-dividing cells reside solely on respiration to produce energy and biomass. Considering the here identified metabolic threshold separating cell division from cell cycle arrest, we envision that the metabolic oscillator and its correlated dynamics may constitute reliable diagnostic markers or therapeutic targets against cancer.

Experimental procedures

Chemicals

All regular chemicals were purchased from Sigma-Aldrich, Acros Organics, Formedium or Merck Milipore. Potassium phthalate monobasic and 3-indoleacetic acid sodium salt (auxin) were purchased from Sigma-Aldrich.

Strains and strain construction

The prototrophic YSBN6 strain, derived from S288c, and its HIS- variant (YSBN16) were used. For an overview on all strains refer to Table S1.

In order to dynamically deplete adenylate cyclase, the central node of the cAMP/PKA pathway, we tagged the respective protein (Cyr1), with the truncated degron sequence $AID^{71\text{-}114}$, previously tested and successfully applied in yeast cells (Morawska and Ulrich,

2013). Flanking sequences adjacent to the stop codon of Cyr1 were amplified using the primers CYR1-CDS and CYR-DOWN. The mCherry coding sequence, together with the truncated degron tag (AID^{71-114}) and the NatMX antibiotic resistance cassette, were amplified in a single piece from the pG23A plasmid (primers mCherry-IAA-Nat). The ampicillin resistance cassette and the ColE1 origin of replication, for selection and amplification into *Escherichia coli*, were amplified in one piece from the pG23A plasmid (primers Amp). The four pieces were assembled into the pG19A plasmid using Gibson assembly (Gibson et al., 2009). The pG19A assembly product was verified by sequencing (primers Seq102, G5NAT & CYR-DOWN Rev), linearized by PCR (primers CYR1Lin) and was used to transform YSBN6 wild type yeast cells, under the selection of ClonNAT. For all yeast transformations we used the lithium acetate high-efficiency protocol (Gietz and Schiestl, 2007). Correct integration into the YSBN6.G19A strain was confirmed using PCR (primers CYR1Lin).

For the deletion of the Rim15 metabolic attenuator, we substituted its coding sequence with the Ble gene, offering resistance to phleomycin. Flanking sequences upstream and downstream the Rim15 coding sequence were amplified using the primers RIM15-UP and RIM15-DOWN, respectively. The Ble antibiotic resistance cassette was amplified from the pG25 plasmid (primers Phleo). The ampicillin resistance cassette and the ColE1 origin of replication, for selection and amplification into *Escherichia coli*, were amplified in one piece from the pG23A plasmid (primers Amp). The four pieces were assembled into the pG27 plasmid using Gibson assembly. The pG27 assembly product was verified by sequencing (primers Phleo Fwd/Rev & Seq6Rev), linearized by PCR (primers RIM15Lin2) and was used to transform YSBN6 wild type and YSBN6.G19A yeast cells, under the selection of ClonNAT. Correct integration into the YSBN6.Rim15Δ and the YSBN6.G19A.Rim15Δ strains was confirmed using PCR (primers RIM15Lin2).

Cultivation

Single yeast colonies growing on YPD 20 gL^{-1} glucose agar plates were used to inoculate 10 mL minimal 10 gL^{-1} glucose medium (pH was adjusted with 10mM K-Phthalate-KOH to pH 5) (Verduyn et al., 1992) in 100 mL shake flasks, and grown (at 30°C, 300 rpm)

overnight. The overnight culture was used to inoculate fresh 10 gL^{-1} glucose medium to an OD of 0.1, which was grown to an OD between 1 and 1.5 (still exponential growth on 10 gL^{-1} glucose).

For microscopy experiments on 10 gL^{-1} glucose, the exponentially growing cells were again diluted to an OD of 0.05 in fresh 10 gL^{-1} glucose medium, and then used to load the microfluidic chip as described (Huberts et al., 2013; Lee et al., 2012). For microscopy experiments on 0.01 gL^{-1} glucose, the exponentially growing cells on 10 gL^{-1} glucose were used to inoculate a 0.01 gL^{-1} glucose medium to an OD of 0.05, and grown to an OD of 0.2 to 0.8. This exponentially growing culture was used to inoculate a fresh 0.01 gL^{-1} glucose medium to an OD of 0.05, where the cells were grown for 2 hours and then used to load the microfluidic chip. In the Cyr1 and Cdc28 depletion experiments, the Cyr1-mCherry-AID or Cdc28-AID expressing cells were always mixed with cells expressing mGFP-AID (YSBN6.G2J - Table S1) to determine the timing of protein depletion (Figures S1 & 2A-B). 0.1 mM of auxin were used in all perturbation experiments, where the auxin-inducible degron was used (AID). During cell culturing in the microfluidic chip, cells were fed at 4.8 μL min-1 with the same media as in the culture before loading. The provided media were pre-warmed to 30°C and saturated with atmospheric air by shaking at 300 rpm for at least two hours prior to use. In alpha factor perturbation experiments, the medium was switched to a medium supplemented with 5 μg mL-1 alpha factor, a previously specified concentration (Futcher, 1999).

For the flow-cytometry experiments, performed on the population level, exponentially growing cells were diluted in fresh, pre-warmed and oxygen saturated minimal medium containing 10gL^{-1} glucose, at an initial OD of 0.1.

Microscopic analyses

Image acquisition (Nikon Ti-E inverted microscopes with either an Andor 897 Ultra EX2 EM-CCD camera or 2x Andror LucaR EM-CCD dual camera system; CoolLed pE2 excitation system; Nikon PFS dynamic focusing system) took place every 5 min (for 10 gL^{-1}) and 10 min (for 0.01 gL^{-1} glucose), in the DIC, NAD(P)H, GFP and RFP channels using

a 40x Nikon Super Fluor Apochromat objective. For the observation of sustained metabolic oscillations in the absence of budding on low glucose, 20 minutes measurement intervals were applied. For NADH measurements, cells were excited at 365 nm with 15% excitation light intensity using a 350/50 nm bandpass filter. The NAD(P)H emission was recorded with no binning using a 409 nm beam-splitter and a 435/40 nm emission filter. For GFP measurements (mGFP-AID and Whi5-eGFP), cells were excited at 470 nm with 15% light intensity using a 470/40 nm bandpass filter. The GFP emission was recorded using a 495 nm beamsplitter and a 525/50 nm emission filter. For the mCherry (Cyr1, mCherry-AID) and mRFP1 (Hta2-mRFP1) measurements, cells were excited at 565 nm with 50% or 15% light intensity respectively, using a 560/40 nm bandpass filter. The mCherry/mRFP1 emission was recorded using a 585 nm beamsplitter and a 630/75 nm emission filter. 200 msec exposure time was applied for the NAD(P)H, GFP and mRFP1 channels, as well as during DIC imaging. 600 msec exposure time was applied for the mCherry channel. In the DIC channel, a halogen lamp was used as a light source, the light of which was filtered through an ultraviolet light filter (420 nm beamsplitter) to minimize cell damage during the long image acquisition. The NIS elements software (LIM) was used to control the microscope and image acquisition.

Image Analysis

For segmentation and tracking of single yeast cells, the BudJ plug-in (Ferrezuelo et al., 2012) for ImageJ (Schneider et al., 2012) was used. The plug-in was used to determine the background-corrected average cytoplasmic pixel fluorescence intensity from single cells, for the GFP (mGFP-AID) and NAD(P)H channels. Specifically, cells to be tracked over time were selected by clicking at the center of the desired cell and their boundaries were estimated by BudJ based on the pixel intensity change at the perimeter of the cell, as visualized in the DIC image. Because of the constitutive filamentation of the Cdc28-AID cells, they were manually segmented on the basis of the cellular borderline in the DIC channel, using ImageJ (Schneider et al., 2012).

The average fluorescence intensity of the pixels contained within the specified cell boundaries was determined for each cell by BudJ for the NAD(P)H channel, and the GFP

channel (mGFP-AID). The modal grey value of the whole image area in each fluorescent channel determined for each time-point was subtracted from the fluorescence of each monitored cell. A comparison of the automated background estimation (i.e. the modal grey value) with a manual background acquisition (average intensity of the pixels around the cell covering the pad area) showed no significant differences between the two methods. For the quantification of the Cyr1-mCherry-AID fluorescence, the cellular auto-fluorescence in the RFP channel was measured in the mGFP-AID cells, and subtracted from the Cyr1-mCherry-AID fluorescence.

The Whi5 nuclear or cytoplasmic localization was manually determined for each single cell. The time point of budding was also manually determined as the moment of first bud appearance on the cell surface, which we monitored in the DIC channel.

Flow cytometry

A BD Accuri flow-cytometer was used to measure the cell count and forward scatter of yeast cells upon the addition of auxin or the mating pheromone alpha factor. Cells were grown in 50 mL (500 mL flask) minimal medium supplemented with $10gL^{-1}$ glucose. At each time, point 25 µl of cell culture at appropriate dilutions to maintain the cell count below 200000 cells / 25 µl, were analyzed.

Ethanol yield estimation

To determine the ethanol yield in the presence or absence of alpha factor, in wild type or *Rim15Δ* cells, the ethanol production and glucose consumption rates were determined. Specifically, 300 µl of culture were sampled in 1.5 ml centrifuge tubes, at each time point. The cells were centrifuged at maximum speed (13000 rpm) for 1 minute and the supernatant was collected. To remove cell traces, the supernatant was additionally filtered through 0.22 µm filter spin-columns (SpinX).

The glucose and ethanol concentrations in the culture supernatant were determined using high performance liquid chromatography (Agilent, isocratic 1290 LC HPLC system) and the Hi-Plex H column, at 60 oC. A flow rate of 0.6 ml/min was applied, with a 5 mM H2SO4 eluent. Appropriate glucose and ethanol concentration standards were prepared and analyzed together with the samples, at the begging and the end of the experiment. The injection volume was set at 10 μl for both the samples and the standards. Substrate concentrations were detected with refractive index and UV (at 210 nm) detection. The chromatogram integration was done with Agilent Open Lab CDS.

Author contributions

AP conceived and designed the study, developed all strains, performed all experiments, and analyzed all data. VT Developed the Cyr1-AID strain. MH conceived and supervised the study. AP and MH wrote the manuscript.

Acknowledgments

Financial support is acknowledged from the EU ITN project ISOLATE. The authors thank the Molecular Systems Biology group for helpful discussion.

References

Bardwell, L. (2004). A walk-through of the yeast mating pheromone response pathway. Peptides 25, 1465–1476.

Baroni, M.D., Monti, P., and Alberghina, L. (1994). Repression of growth-regulated Gl cyclin expression by cyclic AMP in budding yeast. Nature 371, 339–342.

Cai, L., and Tu, B.P. (2012). Driving the cell cycle through metabolism. Annu. Rev. Cell Dev. Biol. 18, 59–87.

Cai, L., Sutter, B.M., Li, B., and Tu, B.P. (2011). Acetyl-CoA Induces Cell Growth and Proliferation by Promoting the Acetylation of Histones at Growth Genes. Mol. Cell 42, 426–437.

Conrad, M., Schothorst, J., Kankipati, H.N., Van Zeebroeck, G., Rubio-Texeira, M., and Thevelein, J.M. (2014). Nutrient sensing and signaling in the yeast *Saccharomyces cerevisiae*. FEMS Microbiol. Rev. 38, 254-299.

Cornelia Amariei, R.M.V.S.T.S.M.T. and D.B.M. (2014). Time resolved DNA occupancy dynamics during the respiratory oscillation uncover a global reset point in the yeast growth program. Microb. Cell 1, 279–288.

Costanzo, M., Nishikawa, J.L., Tang, X., Millman, J.S., Schub, O., Breitkreuz, K., Dewar, D., Rupes, I., Andrews, B., and Tyers, M. (2004). CDK activity antagonizes Whi5, an inhibitor of G1/S transcription in yeast. Cell 117, 899–913.

Deutscher, D., Meilijson, I., Schuster, S., and Ruppin, E. (2008). Can single knockouts accurately single out gene functions? BMC Syst. Biol. 2, 50.

Diaz-Ruiz, R., Rigoulet, M., and Devin, A. (2011). The Warburg and Crabtree effects: On the origin of cancer cell energy metabolism and of yeast glucose repression. Biochim. Biophys. Acta 1807, 568–576.

Ewald, J.C., Kuehne, A., Zamboni, N., and Skotheim, J.M. (2016). The Yeast Cyclin-Dependent Kinase Routes Carbon Fluxes to Fuel Cell Cycle Progression. Mol. Cell 62, 532–545.

Ferrezuelo, F., Colomina, N., Palmisano, A., Garí, E., Gallego, C., Csikász-Nagy, A., and Aldea, M. (2012). The critical size is set at a single-cell level by growth rate to attain homeostasis and adaptation. Nat. Commun. 3, 1–11.

François, J., and Parrou, J.L. (2001). Reserve carbohydrates metabolism in the yeast *Saccharomyces cerevisiae*. FEMS Microbiol. Rev. 25, 125-145.

Futcher, B. (1999). Cell cycle synchronization. Methods Cell Sci. 21, 79–86.

Futcher, B. (2006). Metabolic cycle, cell cycle, and the finishing kick to Start. Genome Biol. 7, 107.

Gibson, D.G., Young, L., Chuang, R.-Y., Venter, J.C., Hutchison, C.A., and Smith, H.O. (2009). Enzymatic assembly of DNA molecules up to several hundred kilobases. Nat Meth 6, 343–345.

Gietz, R.D., and Schiestl, R.H. (2007). High-efficiency yeast transformation using the LiAc/SS carrier DNA/PEG method. Nat. Protoc. 2, 31–34.

Guillou, V., Plourde-Owobi, L., Parrou, J.L., Goma, G., and François, J. (2004). Role of reserve carbohydrates in the growth dynamics of *Saccharomyces cerevisiae*. FEMS Yeast Res. 4, 773-787.

Vander Heiden, M.G., Cantley, L.C., and Thompson, C.B. (2009). Understanding the Warburg Effect: The Metabolic Requirements of Cell Proliferation. Science 324, 1029–1033.

Huberts, D.H.E.W., Lee, S.S., González, J., Janssens, G.E., Vizcarra, I.A., and Heinemann, M. (2013). Construction and use of a microfluidic dissection platform for long-term imaging of cellular processes in budding yeast. Nat. Protoc. 8, 1019–1027.

Jones, R.G., Plas, D.R., Kubek, S., Buzzai, M., Mu, J., Xu, Y., Birnbaum, M.J., and Thompson, C.B. (2016). AMP-Activated Protein Kinase Induces a p53-Dependent Metabolic Checkpoint. Mol. Cell 18, 283–293.

Kotani, S., Tugendreich, S., Fujii, M., Jorgensen, P.-M., Watanabe, N., Hoog, C., Hieter, P., and Todokoro, K. (2016). PKA and MPF-Activated Polo-like Kinase Regulate Anaphase-Promoting Complex Activity and Mitosis Progression. Mol. Cell 1, 371–380.

Lee, I.H., and Finkel, T. (2013). Metabolic regulation of the cell cycle. Curr. Opin. Cell Biol. 25, 724–729.

Lee, P., Kim, M.S., Paik, S.-M., Choi, S.-H., Cho, B.-R., and Hahn, J.-S. (2013). Rim15-dependent activation of Hsf1 and Msn2/4 transcription factors by direct phosphorylation in *Saccharomyces cerevisiae*. FEBS Lett. 587, 3648–3655.

Lee, S.S., Avalos, I., Huberts, D.H.E.W., Lee, L.P., and Heinemann, M. (2012). Whole lifespan microscopic observation of budding yeast aging through a microfluidic dissection platform. Proc. Natl. Acad. Sci. 109, 4916–4920.

Liao, H., and Thorner, J. (1980). Yeast mating pheromone a factor inhibits adenylate cyclase Biochemistry : 77, 1898–1902.

Liu, X., Wang, X., Yang, X., Liu, S., Jiang, L., Qu, Y., Hu, L., Ouyang, Q., and Tang, C. (2015). Reliable cell cycle commitment in budding yeast is ensured by signal integration. Elife 4, e03977.

Lloyd, D., and Murray, D.B. (2005). Ultradian metronome: timekeeper for orchestration of cellular coherence. Trends Biochem. Sci. 30, 373–377.

Lloyd, D., Salgado, L.E.J., Turner, M.P., Suller, M.T.E., and Murray, D. (2002). Cycles of mitochondrial energization driven by the ultradian clock in a continuous culture of *Saccharomyces cerevisiae*. Microbiology 148, 3715–3724.

Machné, R., and Murray, D.B. (2012). The yin and yang of yeast transcription: elements of a global feedback system between metabolism and chromatin. PLoS One 7, e37906.

Mizunuma, M., Tsubakiyama, R., Ogawa, T., Shitamukai, A., Kobayashi, Y., Inai, T., Kume, K., and Hirata, D. (2013). Ras/cAMP-dependent Protein Kinase (PKA) Regulates Multiple Aspects of Cellular Events by Phosphorylating the Whi3 Cell Cycle Regulator in Budding Yeast. J. Biol. Chem. 288, 10558–10566.

Morawska, M., and Ulrich, H.D. (2013). An expanded tool kit for the auxin-inducible degron system in budding yeast. Yeast 30, 341–351.

Müller, D., Exler, S., Aguilera-Vázquez, L., Guerrero-Martín, E., and Reuss, M. (2003). Cyclic AMP mediates the cell cycle dynamics of energy metabolism in *Saccharomyces cerevisiae*. Yeast 20, 351–367.

Nishimura, K., Fukagawa, T., Takisawa, H., Kakimoto, T., and Kanemaki, M. (2009). An auxin-based degron system for the rapid depletion of proteins in nonplant cells. Nat. Methods 6, 917–922.

Papagiannakis, A., Niebel, B., Wit, E.C., and Heinemann, M. (2017). Autonomous metabolic oscillations robustly gate the early and the late cell cycle. Mol. Cell 65, 285–295.

Pedruzzi, I., Bürckert, N., Egger, P., and De Virgilio, C. (2000). *Saccharomyces cerevisiae* Ras/cAMP pathway controls post-diauxic shift element-dependent transcription through the zinc finger protein Gis1. EMBO J. 19, 2569–2579.

Peeters, T., Louwet, W., Geladé, R., Nauwelaers, D., Thevelein, J.M., and Versele, M. (2006). Kelch-repeat proteins interacting with the G(α) protein Gpa2 bypass adenylate cyclase for direct regulation of protein kinase A in yeast. Proc. Natl. Acad. Sci. U. S. A. 103, 13034–13039.

Peters, K. (2013). Molecular mechanisms involved in activation of the Ras proteins by glycolytic flux. Katholieke Universiteit Leuven.

Reinders, A., Bürckert, N., Boller, T., Wiemken, A., and De Virgilio, C. (1998). *Saccharomyces cerevisiae* cAMP-dependent protein kinase controls entry into stationary phase through the Rim15p protein kinase. Genes Dev. 12, 2943–2955.

Sasidharan, K., Soga, T., Tomita, M., and Murray, D.B. (2012). A yeast metabolite extraction protocol optimised for time-series analyses. PLoS One 7, e44283.

Schieke, S.M., McCoy Jr., J.P., and Finkel, T. (2008). Coordination of mitochondrial bioenergetics with G1 phase cell cycle progression. Cell Cycle 7, 1782–1787.

Schmoller, K.M., Turner, J.J., Koivomagi, M., and Skotheim, J.M. (2015). Dilution of the cell cycle inhibitor Whi5 controls budding-yeast cell size. Nature 526, 268–272.

Schneider, C.A., Rasband, W.S., and Eliceiri, K.W. (2012). NIH Image to ImageJ: 25 years of image analysis. Nat Meth 9, 671–675.

Shi, L., and Tu, B.P. (2013). Acetyl-CoA induces transcription of the key G1 cyclin CLN3 to promote entry into the cell division cycle in Saccharomyces cerevisiae. Proc. Natl. Acad. Sci. 110, 7318–7323.

Slavov, N., and Botstein, D. (2011). Coupling among growth rate response, metabolic cycle, and cell division cycle in yeast. Mol. Biol. Cell 22, 1997–2009.

Smith, A., Ward, M.P., and Garrett, S. (1998). Yeast PKA represses Msn2p/Msn4p-dependent gene expression to regulate growth, stress response and glycogen accumulation. EMBO J. 17, 3556–3564.

Talia, S. Di, Skotheim, J.M., Bean, J.M., Siggia, E.D., and Cross, F.R. (2007). The effects of molecular noise and size control on variability in the budding yeast cell cycle. Nature 448, 947–951.

Thevelein, J.M., and de Winde, J.H. (1999). Novel sensing mechanisms and targets for the cAMP-protein kinase A pathway in the yeast Saccharomyces cerevisiae. Mol. Microbiol. 33, 904–918.

Tu, B.P., Kudlicki, A., Rowicka, M., and McKnight, S.L. (2005). Logic of the yeast metabolic cycle: temporal compartmentalization of cellular processes. Science 310, 1152–1158.

Valbuena, N., and Moreno, S. (2010). TOR and PKA Pathways Synergize at the Level of the Ste11 Transcription Factor to Prevent Mating and Meiosis in Fission Yeast. PLoS One 5, e11514.

Verduyn, C., Postma, E., Scheffers, A.W., and van Dijken, J. (1992). Effect of Benzoic Acid on Metabolic Fluxes in Yeasts: A Continuous-Culture Study on the Regulation of Respiration and Alcoholic Fermentation. Yeast 8, 501–517.

Wang, Z., Fan, M., Candas, D., Zhang, T.-Q., Eldridge, A., Wachsmann-Hogiu, S., Ahmed, K.M., Chromy, B.A., Nantajit, D., Duru, N., et al. (2014). CyclinB1/Cdk1 Coordinates Mitochondrial Respiration for Cell Cycle G2/M Progression. Dev. Cell 29, 217–232.

Xu, Z., and Tsurugi, K. (2006). A potential mechanism of energy-metabolism oscillation in an aerobic chemostat culture of the yeast Saccharomyces cerevisiae. FEBS J. 273, 1696–1709.

Zhao, G., Chen, Y., Carey, L., and Futcher, B. (2016). Cyclin-Dependent Kinase Co-Ordinates Carbohydrate Metabolism and Cell Cycle in S. cerevisiae. Mol. Cell 62, 546–557.

Zimmermann, G., Zhou, D., and Taussig, R. (1998). Genetic Selection of Mammalian Adenylyl Cyclases Insensitive to Stimulation by Gsα . J. Biol. Chem. 273, 6968–6975.

Supplemental Information for

CDK and cAMP/PKA signalling tune the amplitude of the metabolic oscillator, thereby controlling cell cycle initiation or arrest

Alexandros Papagiannakis, Vakil Takhaveev, Matthias Heinemann

Molecular Systems Biology, Groningen Biomolecular Sciences and Biotechnology Institute, University of Groningen, Nijenborgh 4, 9747 AG Groningen, The Netherlands;

Supplemental Figures

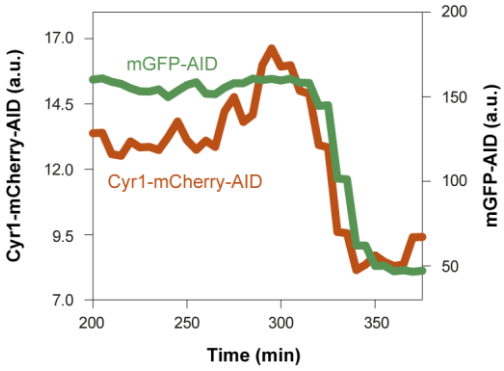

Figure S1: The mGFP-AID depletion dynamics can be used to estimate the timing of Cyr1-AID depletion in the same experiment. Two cell populations, one expressing mGFP-AID and a second population expressing Cyr1-mCherry-AID were loaded in the same microfluidic device and monitored in the same experiment upon the addition of 0.1 mM auxin. The average mGFP-AID depletion (from 13 single cells) was plotted against the average Cyr1-mCherry-AID depletion (from 4 single cells). The depletion dynamics of the two proteins are similar. Both mGFP-AID and Cyr1-mCherry-AID were fully depleted at 350 min. Because the Cyr1-mCherry-AID signal intensity is very low, we used mGFP-AID as reliable reporter for conditional protein depletion.

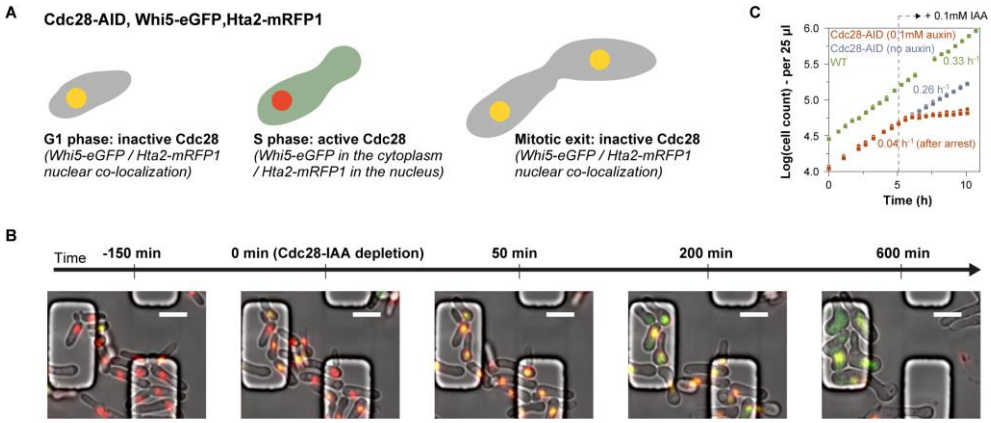

Figure S2: The localization of the transcriptional repressor Whi5 reports CDK activity in single yeast cells. (A) Whi5 is a repressor of cell cycle transcription and is sequestered in the nucleus during the G1 phase or when the cell cycle program is inactive. Whi5 is phosphorylated by Cdc28 and localizes into the cytoplasm at START signalling the initiation of the cell cycle program and reporting CDK activity. To follow the localization of Whi5-eGFP in single cells, we used the fluorescently labelled histone A2 (Hta2-mRFP1) as a nuclear marker. **(B)** Upon the conditional depletion of Cdc28-

AID, the Whi5 transcriptional repressor immediately enters the nucleus, reporting absence of CDK activity. Because yeast cells are not synchronized in the microfluidic device, at the time of Cdc28 depletion they are at different cell cycle phases. Thus we conclude that the cell cycle is arrested at any cell cycle phase. **(C)** The immediate arrest of the cell cycle and growth upon depletion of Cdc28-AID is also visible on the population level. Cell count was measured in batch cultures of wild type cells, and Cdc28-AID cells growing before and after the addition of auxin. The addition of 0.1 mM of auxin at 5.08 hours arrested the growth of Cdc28-AID cells. In the absence of auxin the Cdc28-AID cells grow exponentially, yet with lower growth rate as compared to wild type cells, where the Cdc28 is not tagged. Two biological replicates and their average growth rate are presented for each strain and condition (i.e. presence or absence of auxin). The Cdc28-AID cells exhibit a filamentous phenotype, which explains their slower growth as compared to wild type cells. It has previously been shown that the binding between Cdc28 and its regulatory subunit Cks1 is necessary to prevent filamentous growth of budding yeast. We conclude that the C-terminal tagging of Cdc28 with the auxin degron tag disturbs this interaction inducing constitutive filamentation. This filamentous phenotype we could not avoid even when we tagged the yeast CDK at its N-terminus (strain YSBN16.Whi5-eGFP.Hta2-mRFP1.OsTIR1w/oGFP.G28ARFPex – data not presented).

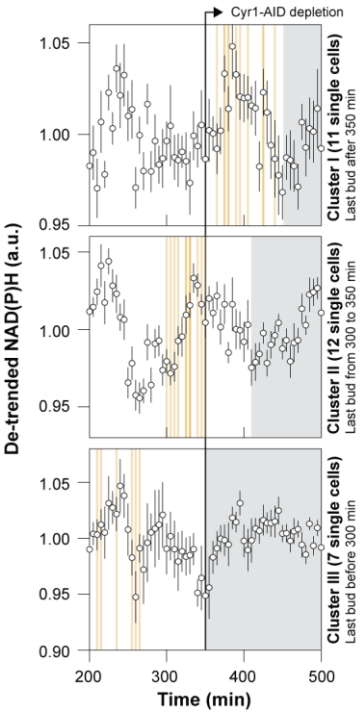

Figure S3: The conditional Cyr1 depletion arrests the cell cycle in G1. Single cells are clustered in 3 groups based on the timing of their last budding (orange vertical lines). The average NAD(P)H dynamics (error bars - SEM) are presented for each cluster. In all three clusters the cells were arrested after the following trough of the NAD(P)H oscillations (grey shaded area). We have previously

shown that the trough of the NAD(P)H oscillations coincide with mitotic exit independently of the nutrient conditions. Thus, upon Cyr1-AID depletion cells are arrested after mitotic exit, or in the G1 phase.

Supplemental Tables

Table S1: Yeast strains developed and/or used in this study.

Strain	Genotype	Source
YSBN6	YSBN6 wild type	Steve Oliver lab, Cambridge
YSBN6.Rim15Δ	YSBN6 Rim15::Ble (deletion)	This study
YSBN6.G19A	YSBN6 Cyr1::mCherry-AID -NatMX	This study
YSBN6.G19A.Rim15Δ	YSBN6 Cyr1::mCherry-AID -NatMX Rim15::Ble (deletion)	This study
YSBN6.G2J	YSBN6 ho::ADH1p-OsTIR1-mGFP-AID -KanMX4	(Papagiannakis et al., 2017)
YSBN6.OsTIR1w/oGFP	YSBN6 ho::ADH1p-OsTIR1-KanMX4	(Papagiannakis et al., 2017)
YSBN16.Whi5-eGFP.Hta2-mRFP1.OsTIR1w/oGFP.G23ARFPex	YSBN16 ho::ADH1p-OsTIR1-KanMX4 Whi5::eGFP-HIS3MX6 Hta2::mRFP1-Ble Cdc14::mCherry-AID$^{71-114}$-natMX	(Papagiannakis et al., 2017)
YSBN16.Whi5-eGFP.Hta2-mRFP1.OsTIR1w/oGFP.G25ARFPex	YSBN16 ho::ADH1p-OsTIR1-KanMX4 Whi5::eGFP-HIS3MX6 Hta2::mRFP1-Ble Cdc28::AID$^{71-114}$-natMX (C-terminal tagging)	(Chapter 3 of this Thesis)

YSBN16.Whi5-eGFP.Hta2-mRFP1.OsTIR1w/oGFP.G28ARFPex	YSBN16 ho::ADH1p-OsTIR1-KanMX4 Whi5::eGFP-HIS3MX6 Hta2::mRFP1-Ble Cdc28::AID$^{71-114}$-natMX (N terminal tagging)	This study

Table S2: Primer sequences used for the development of all recombinant strains.

The underlined sequences correspond to the overhangs designed for Gibson assembly. The term "gDNA" stands for purified genomic DNA.

Primer	Fwd/Rev	Sequence (5′ to 3′)	Templates
CYR1CDS	Fwd	TTATGCTTCCGCGGCTCGTATGTTGTGTGGGTATTGGTTGGGCATTTTTTGACTT	YSBN6 wild type gDNA
	Rev	CATGTTATCCTCCTCGCCCTTGCTCACCATAGTTGATAAATCCTTTGCGTTCTTAAC	
CYR1 DOWN	Fwd	CCGGGTGACCCGGCGGGGACAAGGCAAGCTGTTCTGTTCGTAAATTATGTACCACC	
	Rev	GTTCCAGTTTGGAACAAGAGTCCACTATTAGAGAGAGCTTAGAGACACCTTTT	
RIM15 UP	Fwd	TTATGCTTCCGCGGCTCGTATGTTGTGTGGCATTTCTCGAGTTGTCCATTGAG	
	Rev	GTCGAAAACGAGCTCTCGAGAACCCTTAATCTGTCTTCCTCTACTGGGC	
RIM15 DOWN	Fwd	CGAGGCAAGCTAAACAGATCTCTAGACCTAGCGATTCTGATGAAACGCAC	
	Rev	GTTCCAGTTTGGAACAAGAGTCCACTATTAGGAAGTGGAATCATCAAACGAC	
mCherry-IAA-Nat	Fwd	ATGGTGAGCAAGGGCGA	pG23A plasmid (Papagiannakis et
	Rev	AGCTTGCCTTGTCCCCG	

Amp	Fwd	TAATAGTGGACTCTTGTTCC	al., 2017)
	Rev	CCACACAACATACGAGC	
Phleo Phleo	Fwd	ATTAAGGGTTCTCGAGAGC	pG25 plasmid (Papagiannakis et al., 2017) pG27 plasmid (This study)
	Rev	TAGGTCTAGAGATCTGTTTAGC	
RIM15Lin	Fwd	CATTTCTCGAGTTGTCCATTGAG	pG27 plasmid (This study)
	Rev	GGAAGTGGAATCATCAAACGAC	
Seq102	Rev	CTTCAGGTTGTCTAACTCC	pG19A (This study)
G5NAT	For	GTCGACGGTGCAGG	
CYR1Lin	For	GTATTGGTTGGGCATTTTTTG	
	Rev	GAGAGAGCTTAGAGACACC	

Supplemental References

Papagiannakis, A., Niebel, B., Wit, E.C., and Heinemann, M. (2017). Autonomous metabolic oscillations robustly gate the early and the late cell cycle. Mol. Cell 65, 285–295.